A Computational Model for Sound Field Absorption by Acoustic Arrays

H. T. Banks [*] D. G. Cole [‡] K. M. Furati [*†] K. Ito [*] G. A. Pinter [§]

Rev 6, July 24, 2001

Abstract

In this paper we discuss the sound absorption property of arrays of micro-acoustic actuators at a control surface. We use the wave equation over the half plane for the velocity potential with a boundary dissipation by a proportional pressure feedback law along the half plane boundary. The feedback gain over the array is described by a distributed shape function. We develop a computational method based on the Fourier transform and employ it for analyzing and evaluating the decay rate of acoustic energy. Specifically, we carry out computations for a diffusive random initial field and report on our resulting numerical findings.

1 Introduction

The rise and decay of acoustic energy in a room of a given size is primarily governed by the area and absorption coefficient of the surfaces of the room and objects within [7, 10, 14]. The absorption coefficient of a material with normalized input impedance $\zeta = \theta + i\chi$ is

$$\alpha = \frac{4\theta}{(\theta+1)^2 + \chi^2}. \tag{1}$$

[*]Center for Research on Scientific Computation, Box 8205, NCSU, Raleigh, NC 27695-8205

[†]Department of Mathematical Sciences, KFUPM, Dhahran 31261, Saudi Arabia

[‡]Thomas Lord Research Center, Lord Corporation, Cary, NC 27513

[§]Department of Mathematical Sciences, University of Wisconsin-Milwaukee, Milwaukee, WI 53201-0413

The sound absorbing characteristics of passive materials are excellent when the wavelength of sound is less than the material thickness, because the input impedance is largely resistive. However, as the wavelength of sound increases, the reactive part, χ, of the impedance increases, and the performance of sound absorbing materials decreases drastically [6]. The apparent solution of increasing the area and thickness of absorption treatments is often limited by practical considerations including cost.

Active sound absorbers provide an alternative technique for achieving sound absorption at long wavelengths where the size of the absorber is on the order of the wavelength of sound [5, 8, 11]. Typical active sound absorbers are coupled discrete devices or systems, for example, a system composed of a microphone, speaker, and appropriate control law. The most significant limitation of active sound absorbers is their limited surface area, and again practical consideration limit their use.

Recently the concept of using arrays of small acoustic sources, which could be constructed of fluidic devices [1] or piezoelectric materials, for sound absorption has been of interest. In such an array, each element would be locally reacting by feeding back a pressure measurement via an appropriate compensator to the elemental acoustic source. The dimensionality of an array of practical size, however, limits the analysis of the array's characteristics, including absorption, using techniques used in previous active sound absorber analyses.

In this investigation we develop a computational technique for analyzing the absorption rate of acoustic arrays. Specifically, we consider the absorption rate of an ideal reverberant random sound field as defined in Section 3.

We begin with a brief description of the physical system under consideration, and consider a typical rate feedback law along the boundary where the elemental acoustic source's volume velocity is proportional to the measured pressure at that element. This corresponds to a purely resistive input impedance. We then formulate the acoustic wave equation with the absorption boundary coefficient in the frequency domain. In Section 3 we describe the initial sound field. In Sections 4 and 5 we formulate the system in the frequency domain and obtain a discrete model approximation. Based on this discrete model, in Sections 6 and 7 we show how to calculate the instantaneous correlation field and energy decay. Finally, we report on a numerical experiment and analyze the results.

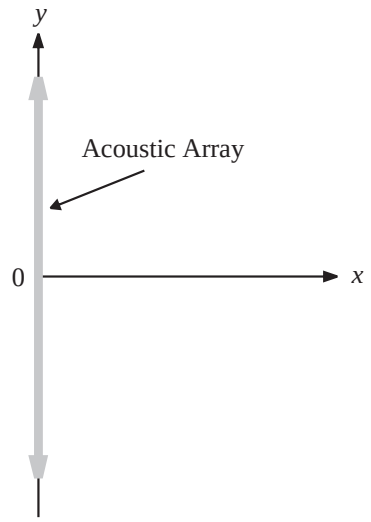

Figure 1: Acoustic array.

2 Physical Problem Equations

In this section we present the physical system under consideration. The sound pressure p satisfies the acoustic wave equation

$$p_{\tau\tau} - c^2\nabla^2 p = 0, \tag{2}$$

and Euler's equation

$$\rho \mathbf{v}_\tau = -\nabla p, \tag{3}$$

where c is the speed of sound in air and ρ is the mass density of air. The operator ∇ is the gradient, $\mathbf{v} = (u, v, w)$ is the particle velocity vector of air, τ denotes time, and $\mathbf{v}_\tau = \partial \mathbf{v}/\partial \tau$; see [4] and [13].

Consider an infinite air space bounded by an infinite rigid wall located at $x = 0$ covered by an acoustic array symmetric about the origin. We assume that the acoustic array is long enough in the z-direction that the system is independent of z and becomes two dimensional, as depicted in Figure 1. Accordingly, our working space is $\Omega = \{(x, y) : x \geq 0, y \in \Re\}$.

The interaction of a wave with the boundary is described by the boundary condition

$$\mathbf{v}(0, y, \tau) \cdot \vec{\imath} = u(0, y, \tau) = -g(y)p(0, y, \tau), \qquad -\infty < y < \infty, \tau > 0. \tag{4}$$

This boundary condition follows from the definition of the *normal input admittance*, the ratio of the particle

velocity normal to the wall to the pressure [6], where g is the interaction admittance. Note for the case of a rigid boundary, $g \equiv 0$, while for a pressure release boundary we have $g \to \infty$.

Let ϕ be the velocity potential, $\mathbf{v} = \nabla\phi$. Then from (3) we have $p = -\rho\phi_\tau$ and it follows from (2) and (4) that ϕ satisfies

$$\phi_{\tau\tau} - c^2\nabla^2\phi = 0 \qquad \text{in } \Omega, \tag{5}$$

$$\phi_x(0, y, \tau) = \rho\, g(y)\, \phi_\tau(0, y, \tau), \qquad -\infty < y < \infty, \tau > 0. \tag{6}$$

We normalize time by the sound speed, letting $t = c\tau$, and we define $\gamma(y) = \rho c\, g(y)$, then (5) and (6) take the form

$$\phi_{tt} - \nabla^2\phi = 0 \qquad \text{in } \Omega \tag{7}$$

$$\phi_x(0, y, t) = \gamma(y)\, \phi_t(0, y, t), \qquad -\infty < y < \infty, t > 0. \tag{8}$$

The admittance magnitude in a given direction is a function of the wave propagation angle. Let $\mathbf{x}$ and $\mathbf{k}$ denote the position vector (x, y) and the wavenumber vector (k, l), respectively. Then for a plane wave, $\phi(\mathbf{x}, t) = \phi_o\, e^{i(\omega t - \mathbf{k}\cdot\mathbf{x})}$, the normalized wave admittance in the x-direction is

$$\beta = \rho c \frac{u}{p} = \frac{k}{\omega} = \frac{k}{|\mathbf{k}|}, \tag{9}$$

since $\omega = |\mathbf{k}|$. We note that $0 \le |\beta| \le 1$ with $|\beta| = 0$ corresponding to a plane wave traveling only in the y-direction and $|\beta| = 1$ corresponding to a plane wave traveling only in the x-direction. In order to absorb sound at the boundary we might choose the normal input admittance γ to match the normal wave admittance β. However, in general, the knowledge of the angle of incidence of the incoming wave is not available. Moreover, for some fields the angle of incidence is arbitrary. For this reason, in our model we test the absorption characteristics for a given γ by the absorption rate of an ideal reverberant sound field where the angle of incidence is uniformly distributed among all directions.

3 Initial Field

The sound field in a reverberation room is assumed to have the property that it is random and at every point within the field all directions of the incoming sound wave are uniformly distributed [3, 9, 12]. The reverberation room has become an important tool in applied acoustics. For example, it is useful in measuring the sound absorption coefficients of surface materials and the sound transmission loss of building structures. Thus in our investigation we assume the initial sound field to be random and the spatial autocorrelation to be independent of the position of the phase and a function of the distance only. That is, the initial random field $\phi(\mathbf{x}, 0)$ satisfies

$$\mathcal{E}\left[\phi(\mathbf{x}, 0)\ \phi(\mathbf{x}+\mathbf{r}, 0)\right] = R(|\mathbf{r}|),$$

for all $\mathbf{x}$, where $\mathcal{E}[\cdot]$ denotes the expectation.

Let $\hat{\phi}(\mathbf{k}, 0)$ be the Fourier transform of $\phi(\mathbf{x}, 0)$,

$$\hat{\phi}(\mathbf{k}, 0) = \int e^{-i\mathbf{k}\cdot\mathbf{x}}\ \phi(\mathbf{x}, 0) d\mathbf{x}.$$

Then, as in [4], the frequency autocorrelation for $\hat{\phi}(\mathbf{k}, 0)$ is given by

$$\mathcal{E}\left[\overline{\hat{\phi}(\mathbf{k}, 0)}\ \hat{\phi}(\mathbf{k}', 0)\right] = (2\pi)^2\ \delta(\mathbf{k}-\mathbf{k}') \int R(|\mathbf{r}|)\ e^{-i\mathbf{k}\cdot\mathbf{r}}\ d\mathbf{r}, \tag{10}$$

where δ is the Dirac delta function.

In this paper we develop approximate methods to evaluate the frequency autocorrelation for the sound field,

$$\mathcal{E}\left[\overline{\hat{\phi}(\mathbf{k}, t)}\ \hat{\phi}(\mathbf{k}', t)\right],$$

for the pressure field,

$$\mathcal{E}\left[\overline{\hat{\phi}_t(\mathbf{k}, t)}\ \hat{\phi}_t(\mathbf{k}', t)\right],$$

and for the velocity field,

$$\mathcal{E}\left[\overline{\nabla\hat{\phi}(\mathbf{k}, t)}\ \nabla\hat{\phi}(\mathbf{k}', t)\right],$$

as well as the total energy decay of the sound field for $t > 0$.

4 Frequency Domain Equations

In this section we reformulate Equation (7) and (8) in the frequency domain. Since the spatial domain Ω is the half plane $x > 0$, then without loss of generality we use the Fourier cosine transform with respect to x and full Fourier transform with respect to y. Let $\hat{\phi}$ be the Fourier cosine-full transform of ϕ,

$$\hat{\phi}(\mathbf{k}, t) = \hat{\phi}(k, l, t) = \int_{-\infty}^{\infty} \int_{0}^{\infty} \phi(x, y, t) \cos(kx)\, e^{-ily}\, dx\, dy. \tag{11}$$

Then the inverse transform is given by

$$\phi(\mathbf{x}, t) = \phi(x, y, t) = \frac{1}{\pi^2} \int_{-\infty}^{\infty} \int_{0}^{\infty} \hat{\phi}(k, l, t) \cos(kx)\, e^{ily}\, dk\, dl. \tag{12}$$

We can derive an equation for $\hat{\phi}(k, l, t)$ as follows. We multiply (7) by $\cos(kx)e^{-ily}$, and apply Green's Formula and (8) to obtain

$$\begin{aligned} &\partial_{tt} \int_{-\infty}^{\infty} \int_{0}^{\infty} \phi(x, y, t) \cos(kx)\, e^{-ily}\, dx\, dy = \\ &-(k^2 + l^2) \int_{-\infty}^{\infty} \int_{0}^{\infty} \phi(x, y, t) \cos(kx)\, e^{-ily}\, dx\, dy - \int_{-\infty}^{\infty} \gamma(y) \phi_t(0, y, t)\, e^{-ily}\, dy. \end{aligned} \tag{13}$$

Then, by applying the formulas (11) and (12) we can write (13) as

$$\hat{\phi}_{tt}(k, l, t) = -(k^2 + l^2)\hat{\phi}(k, l, t) - \int_{-\infty}^{\infty} \int_{0}^{\infty} \hat{\phi}_t(\alpha, \beta, t)\, \hat{\gamma}(l, \beta)\, d\alpha\, d\beta, \tag{14}$$

where

$$\hat{\gamma}(l, \beta) = \frac{1}{\pi^2} \int_{-\infty}^{\infty} \gamma(y) e^{-i(l-\beta)y}\, dy.$$

Since the acoustic array is assumed to be symmetric, $\gamma(y)$ is an even function and thus

$$\hat{\gamma}(l, \beta) = \frac{2}{\pi^2} \int_{0}^{\infty} \gamma(y) \cos[(l - \beta)y]\, dy = \frac{2}{\pi^2} \int_{0}^{\infty} \gamma(y)[\cos(ly)\cos(\beta y) + \sin(ly)\sin(\beta y)]\, dy. \tag{15}$$

If we further assume that the initial field is an even function of y, then the map $y \to \phi(\cdot, y, \cdot)$ is even, and we only need to work with the nonnegative values of l. Moreover, the integrand $\gamma(y)\sin(ly)\sin(\beta y)$ in (15) is an odd function of β and thus does not contribute to the integral term of (14). As a result, Equation (14) reduces to

$$\hat{\phi}_{tt}(k, l, t) = -(k^2 + l^2)\hat{\phi}(k, l, t) - \int_{0}^{\infty} \int_{0}^{\infty} \hat{\phi}_t(\alpha, \beta, t)\, \Gamma(l, \beta)\, d\alpha\, d\beta, \tag{16}$$

where

$$\Gamma(l,\beta) = \frac{4}{\pi^2}\int_0^\infty \gamma(y)\cos(ly)\cos(\beta y)\,dy. \tag{17}$$

We note that this yields an integro partial differential equation for $\hat{\phi}$ for which approximation techniques must be developed. In the next section we present a semi-discrete finite element approximation based on piecewise constant elements (zero-order splines).

5 Approximate Model

In this section we introduce a finite dimensional approximation of Equation (16). We consider the truncated finite domain

$$\{(k,l) : 0 \le k \le K, 0 \le l \le L\}. \tag{18}$$

Let $0 = k_0 < k_1 < k_2 < \ldots < k_{_M} = K$ and $0 = l_0 < l_1 < l_2 < \ldots < l_{_N} = L$ be partitions along the k- and l-axis in the kl-plane. Let $\Delta k_i = k_i - k_{i-1}$, $\Delta l_j = l_j - l_{j-1}$, and $R_{ij} = (k_{i-1}, k_i] \times (l_{j-1}, l_j]$. Let $(\tilde{k}_i, \tilde{l}_j)$ denote the midpoint of each cell R_{ij}.

We apply the (piecewise constant in frequency) approximation

$$\hat{\phi}(k,l,t) \approx \Phi^{MN}(k,l,t) = \sum_{i=1}^{M}\sum_{j=1}^{N} \Phi_{ij}^{MN}(t)\chi_{ij}^{MN}(k,l). \tag{19}$$

where

$$\chi_{ij}^{MN}(k,l) = \begin{cases} 1 & (k,l) \in R_{ij}, \\ 0 & \text{otherwise}, \end{cases}$$

and $\Phi_{ij}^{MN}(t)$ is an approximation of $\hat{\phi}(\tilde{k}_i, \tilde{l}_j, t)$. Then, we evaluate (19) at the midpoint of each cell R_{ij}. This results in the system of equations of the form

$$\ddot{\Phi}_{ij}^{MN}(t) + \lambda_{ij}^2 \Phi_{ij}^{MN}(t) + \sum_{n=1}^{N}\left(g_{jn}^{MN} \sum_{m=1}^{M} \Delta k_m \dot{\Phi}_{mn}^{MN}(t)\right) = 0, \tag{20}$$

where

$$\lambda_{ij} = \sqrt{\tilde{k}_i^2 + \tilde{l}_j^2}, \qquad g_{jn}^{MN} = \int_{l_{n-1}}^{l_n} \Gamma(\tilde{l}_j, \beta) d\beta. \tag{21}$$

Note that we should use the superscript MN with the variables in (20) since they depend on the discretization in (k,l). However, for notational convenience, we will hereafter suppress this superscript whenever no confusion will result.

To write this system is the matrix form we introduce the $\Re^{MN}$ vector

$$\Phi = [\Phi_{11}, \Phi_{21}, \ldots, \Phi_{M1}, \Phi_{12}, \Phi_{22}, \ldots, \Phi_{M2}, \ldots, \Phi_{1N}, \Phi_{2N}, \ldots, \Phi_{MN}]^T,$$

the $MN \times MN$ diagonal matrix

$$\Lambda = \text{ diag}(\lambda_{11}^2, \lambda_{21}^2, \ldots, \lambda_{M1}^2, \lambda_{12}^2, \lambda_{22}^2, \ldots, \lambda_{M2}^2, \ldots, \lambda_{1N}^2, \lambda_{2N}^2, \ldots, \lambda_{MN}^2), \tag{22}$$

and the damping matrix

$$G = \begin{bmatrix} g_{11} & g_{12} & \cdots & g_{1N} \\ g_{21} & g_{22} & \cdots & g_{2N} \\ \vdots & \vdots & \cdots & \vdots \\ g_{N1} & g_{N2} & \cdots & g_{NN} \end{bmatrix}. \tag{23}$$

We define the $M \times M$ matrix

$$\Delta_k = \begin{bmatrix} \Delta k_1 & \Delta k_2 & \cdots & \Delta k_M \\ \Delta k_1 & \Delta k_2 & \cdots & \Delta k_M \\ \vdots & \vdots & \cdots & \vdots \\ \Delta k_1 & \Delta k_2 & \cdots & \Delta k_M \end{bmatrix},$$

and let D be the Kronecker tensor product

$$D = \text{ kron}(G, \Delta_k).$$

Then, the second order system (20) can thus be written in the matrix form

$$\ddot{\Phi}(t) + D\dot{\Phi}(t) + \Lambda\Phi(t) = 0. \tag{24}$$

As usual, we can write (24) as a first order system. To that end, define the state vector

$$Z(t) = \begin{bmatrix} \Phi(t) \\ \hline \dot{\Phi}(t) \end{bmatrix}.$$

Then (24) takes the form

$$\dot{Z} = AZ, \tag{25}$$

where A is the $(2MN) \times (2MN)$ matrix defined by

$$A = \left[\begin{array}{c|c} 0 & I \\ \hline -\Lambda & -D \end{array}\right],$$

and I is the $(MN) \times (MN)$ identity matrix. It is this approximate system that we use in our calculations reported on below.

6 Instantaneous Correlation Field

According to the discretization described in Section 5, it follows from (10) that a natural condition to require on the approximating random Fourier components $\{Z_i(0)\}$ is

$$\mathcal{E}\left[Z_i(0)\, Z_j(0)\right] = 0, \quad \text{if } i \neq j. \tag{26}$$

Define the corresponding approximate correlation matrix

$$C(t) = \mathcal{E}\left[Z(t)\, Z^T(t)\right]. \tag{27}$$

Then (26) implies that $C(0)$ is diagonal. Thus, we can write

$$C(0) = \sum_{\nu=1}^{2MN} w_\nu\, e^{(\nu)} \left(e^{(\nu)}\right)^T, \tag{28}$$

where $e^{(\nu)}$ is the unit vector in $\Re^{2MN}$ and $W = (w_\nu)$ is the vector of the initial field discrete power spectral densities.

From (25) and (27) we find that $C(t)$ satisfies the matrix Lyapunov differential equation system

$$\dot{C}(t) = A\, C(t) + C(t)\, A^T. \tag{29}$$

Note that C is a $2MN \times 2MN$ matrix and thus we have a system of size $(2MN)^2$.

The system (29) is a large coupled system to be solved in its entirety. However the solution of (29) is given by

$$C(t) = \sum_{\nu=1}^{2MN} w_\nu\, F^{(\nu)}(t) \left(F^{(\nu)}(t)\right)^T, \tag{30}$$

where the vector $F^{(\nu)}(t)$ for each ν satisfies

$$\dot{F}^{(\nu)}(t) = A\,F^{(\nu)}(t), \qquad F^{(\nu)}(0) = e^{(\nu)}. \tag{31}$$

This can be shown as follows:

$$\begin{aligned}
\dot{C} &= \sum_{\nu=1}^{2MN} w_\nu \left\{ \dot{F}^\nu \left(F^{(\nu)}\right)^T + F^{(\nu)} \left(\dot{F}^\nu\right)^T \right\} \\
&= \sum_{\nu=1}^{2MN} w_\nu \left\{ AF^{(\nu)} \left(F^{(\nu)}\right)^T + F^{(\nu)} \left(AF^{(\nu)}\right)^T \right\} \\
&= \sum_{\nu=1}^{2MN} w_\nu \left\{ AF^{(\nu)} \left(F^{(\nu)}\right)^T + F^{(\nu)} \left(F^{(\nu)}\right)^T A^T \right\} \\
&= A\,C + C\,A^T.
\end{aligned}$$

The superposition formula (30) is especially efficient when we consider fields with compact support Fourier components.

7 Instantaneous Total Energy

We define the total energy of system (24) by

$$E^{MN}(t) = E_V^{MN}(t) + E_P^{MN}(t), \tag{32}$$

where the "kinetic" energy and "potential" energy are given, respectively, by

$$E_V^{MN}(t) = \frac{1}{2}\int \left|\nabla \phi^{MN}(\mathbf{x},t)\right|^2 d\mathbf{x}, \qquad E_P^{MN}(t) = \frac{1}{2}\int \left[\phi_t^{MN}(\mathbf{x},t)\right]^2 d\mathbf{x},$$

and $\phi^{MN}(\mathbf{x},t)$ is the inverse Fourier transform of $\Phi^{MN}(\mathbf{k},t)$ defined in (19). By Parseval's theorem, we have

$$E_V(t) = \frac{1}{2}\Phi^T(t)\,\Lambda\,\Phi(t), \qquad E_P(t) = \frac{1}{2}\dot{\Phi}^T(t)\,\dot{\Phi}(t).$$

We remark that E_V^{MN} is an approximate measure of the kinetic energy density associated with the velocity field while the term E_P^{MN} is an approximate measure of the potential energy density due to the pressure.

Now, by multiplying (24) by $\dot{\Phi}$ we can show that

$$\dot{E}(t) = -\dot{\Phi}^T(t)\,D\,\dot{\Phi}(t) \le 0. \tag{33}$$

We thus see from (33) that the system is dissipative for positive γ.

To describe the relation between the total energy E and the correlation matrix C, we define the matrix

$$\mathcal{L} = \left[\begin{array}{c|c} \sqrt{\Lambda} & 0 \\ \hline 0 & I \end{array}\right].$$

Then from (27) we have

$$\mathcal{L}\,C\,\mathcal{L} = \mathcal{E}\left[\begin{array}{c|c} (\sqrt{\Lambda}\Phi)(\sqrt{\Lambda}\Phi)^T & \sqrt{\Lambda}\Phi\dot{\Phi}^T \\ \hline \dot{\Phi}(\sqrt{\Lambda}\Phi)^T & \dot{\Phi}\dot{\Phi}^T \end{array}\right],$$

and thus

$$\mathcal{E}\,[E(t)] = \frac{1}{2}\,\mathcal{E}\left[\Phi^T(t)\,\mathcal{L}\,\Phi(t) + \dot{\Phi}^T(t)\,\dot{\Phi}(t)\right] = \frac{1}{2}\,\mathrm{trace}[\mathcal{L}\,C(t)\,\mathcal{L}]. \tag{34}$$

Our goal is to quantify the decay mechanism of the total energy as $t \to \infty$. By integrating (31) numerically we can evaluate $F^{(\nu)}(t)$ and determine the decay rate of each mode. Moreover, we can form the correlation matrix C and determine the decay rate of a field composed of a group of modes.

8 Numerical Implementation and Results

In this section we demonstrate how the above approximations and resulting computational model can be used to investigate the energy decay rate of a given bandwidth of velocity pseudo-modes defined by (31).

Consider the periodic acoustic array of length $2L_a$ in the y-direction and symmetric about the origin as depicted in Figure 2. The array consists of elements each of width w. Because of symmetry, we only need to consider the upper half of the array. The number of elements in the half array is given by

$$N_e = L_a/\mathrm{w}.$$

For $n = 1, \ldots N_e$, each nth element occupies the interval $\mathcal{I}_n = [(n-1)\mathrm{w}, n\mathrm{w}]$.

In each element we take the function $\gamma(y)$ to be a symmetric triangle curve of height h as shown in Figure 2. Thus we have

$$\gamma(y) = \begin{cases} \gamma^n(y), & y \in \mathcal{I}_n, \\ 0 & y > L_a, \end{cases}$$

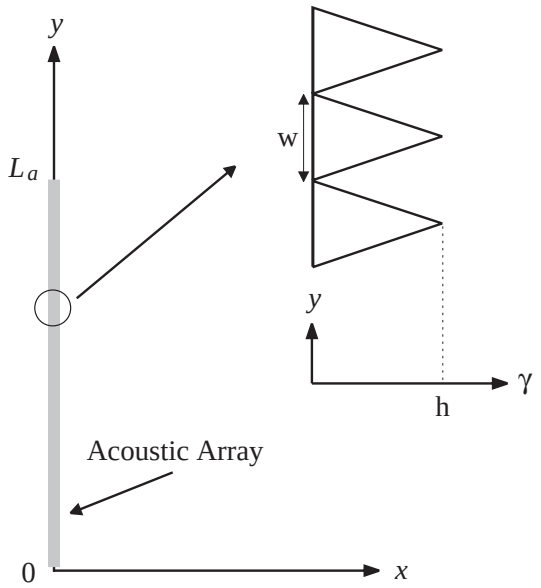

Figure 2: Acoustic array and the admittance function $\gamma(y)$.

where

$$\gamma^n(y) = \begin{cases} \frac{2\mathrm{h}}{\mathrm{w}} y - 2(n-1)\mathrm{h}, & y \in [(n-1)\mathrm{w}, (n-.5)\mathrm{w}], \\ -\frac{2\mathrm{h}}{\mathrm{w}} y + 2n\mathrm{h}, & y \in [(n-.5)\mathrm{w}, n\mathrm{w}]. \end{cases}$$

For our example calculations we use $L_a = 4$ meters and element width $\mathrm{w} = 0.01$ meters. For the height, h, we choose the value 2. For this value, the average value of γ in each element is 1.

Take $K = L = 10$ and uniform partition $\Delta k_i = \Delta l_j = 1$. This implies that $M = N = 10$ and that A of (25) is of size 200×200. We calculate the entries of the matrix G by using the midpoint approximation

$$g_{jn} \approx \Delta l\, \Gamma(\tilde{l}_j, \tilde{l}_n) \ = \frac{4}{\pi^2} \Delta l \int_0^{L_a} \gamma(y) \cos(\tilde{l}_j y) \cos(\tilde{l}_n y)\, dy, \tag{35}$$

and then a quadrature rule, for example, the Trapezoidal rule. Figure 3 depicts the eigenvalues of the resulting matrix A.

As an example, we consider the bandwidth $3.5 \leq |\mathbf{k}| \leq 4.5$. The discrete modes that belong to this bandwidth are shown in Figure 4. The set of these modes is

$$\Upsilon = \{(\tilde{k}_i, \tilde{l}_j) = (\, i - .5, j - .5\,) : (i,j) = (4,1), (4,2), (3,3), (4,3), (1,4), (2,4), (3,4)\}.$$

We assume that the initial field consists only of the velocity field. Thus for the modes in Υ the corresponding

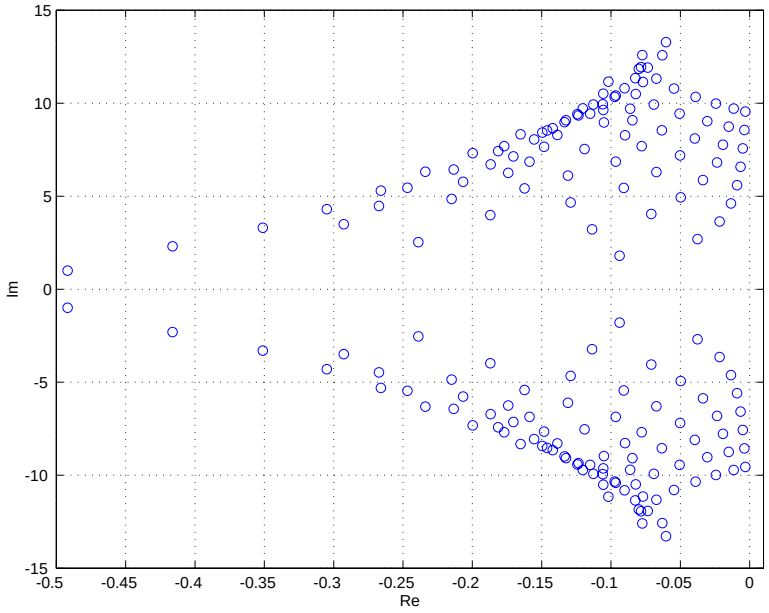

Figure 3: Eigenvalues of the matrix A.

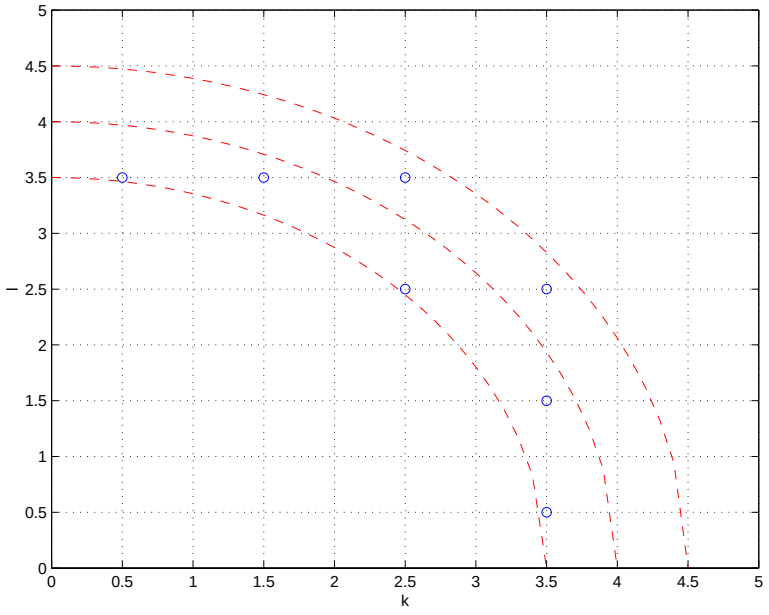

Figure 4: The set Υ of the initial discrete modes.

set of $\nu = i + 10(j-1)$ values is

$$\mathcal{N} = \{4, 14, 23, 24, 31, 32, 33\},$$

and for the coefficients w_ν we have

$$w_\nu = 0, \qquad \nu \notin \mathcal{N},$$

while w_ν, $\nu \in \mathcal{N}$, are given magnitudes that describe the initial field.

As a result, the initial correlation matrix (28) reduces to

$$C^{\mathcal{N}}(0) = \sum_{\nu \in \mathcal{N}} w_\nu e^{(\nu)} \left(e^{(\nu)}\right)^T,$$

and the corresponding instantaneous correlation matrix is given by

$$C^{\mathcal{N}}(t) = \sum_{\nu \in \mathcal{N}} w_\nu F^{(\nu)}(t) \left(F^{(\nu)}(t)\right)^T,$$

where $F^{(\nu)}$ is the pseudo-mode given by (31).

To find $C^{\mathcal{N}}(t)$ we integrate numerically equation (31) for each $F^{(\nu)}$, $\nu \in \mathcal{N}$. We use the MATLAB function `ode23s` which is suitable for the stiff system (31) Once $C^{\mathcal{N}}$ is calculated, then from (34), the corresponding expected instantaneous total energy $E^{\mathcal{N}}$ is given by

$$\mathcal{E}\left[E^{\mathcal{N}}(t)\right] = \frac{1}{2} \operatorname{trace}[\mathcal{L}\, C^{\mathcal{N}}(t) \mathcal{L}]. \tag{36}$$

For simplicity we consider a uniform initial energy distribution of magnitude one for each mode $\nu \in \mathcal{N}$. This implies that

$$w_\nu = \lambda_\nu^{-2} = \lambda_{ij}^{-2}, \qquad \nu \in \mathcal{N},$$

where

$$i = \operatorname{ind}(\nu, 10), \qquad j = (\nu - i)/10 + 1. \tag{37}$$

Here $\operatorname{ind}(a, b)$ is defined as

$$\operatorname{ind}(a,b) = \begin{cases} b & \text{if } b \text{ is a divisor of } a \\ a - [[a/b]] \times b & \text{otherwise} \end{cases}$$

where $[[\cdot]]$ is the greatest integer function.

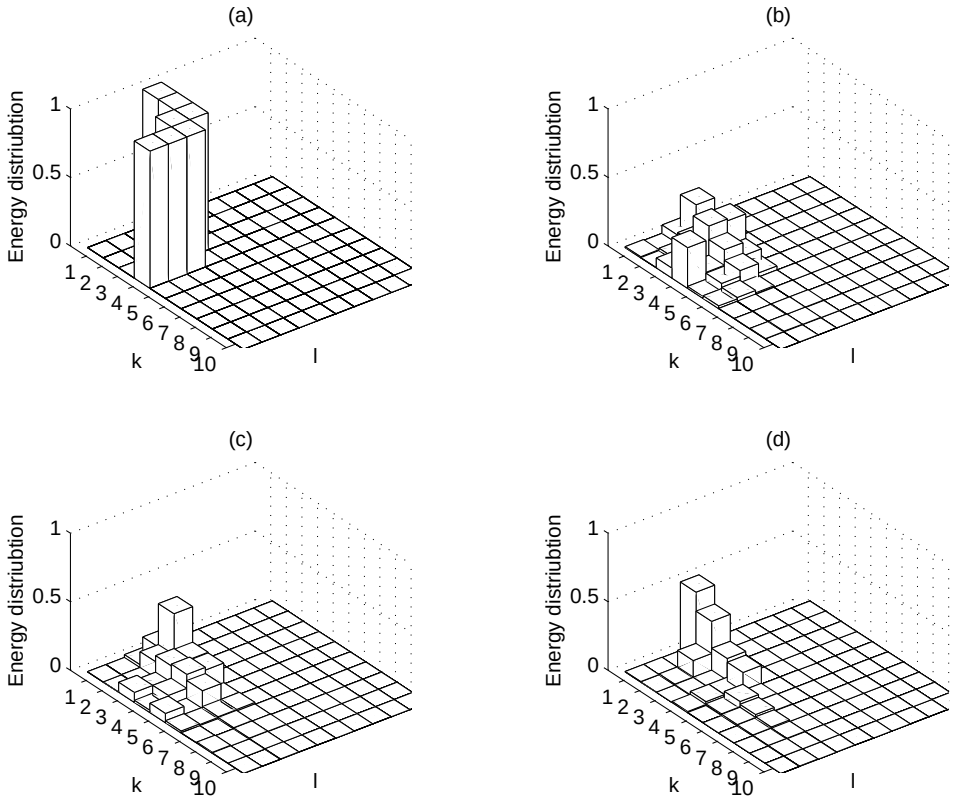

Figure 5: Evolution of the energy distribution matrix $\Xi(t)$ at $t = 0, 2, 4, 6$, depicted in (a), (b), (c), and (d), respectively.

Since $C^{\mathcal{N}}(t)$ has 200×200 entries, it is not convenient to consider a graph that shows the simultaneous evolution of all the entries. However, since the significant interactions take place along the diagonal entries of $C^{\mathcal{N}}$, it will be sufficient to consider these entries only. To visualize the evolution of the correlation matrix associated with velocity field we consider the entries $\left\{\left(\mathcal{L}\, C^{\mathcal{N}}(t)\, \mathcal{L}\right)_{ii}\right\}_{i=1}^{100}$. We form the 10×10 energy distribution matrix $\Xi^{\mathcal{N}}(t)$ by mapping these entries into the kl-space. In Figure 5(a-d) we present the bar graph of the matrix $\Xi^{\mathcal{N}}(t)$ at $t = 0, 2, 4, 6$, respectively. The solid curve in Figure 6 represents the normalized energy

$$10\ \log_{10}\left(\frac{\mathcal{E}\left[E^{\mathcal{N}}(t)\right]}{\mathcal{E}\left[E^{\mathcal{N}}(0)\right]}\right).$$

By examining the eigenvectors of A, we find that each one has a leading entry of maximum magnitude. This enables us to associate each eigenmode with a pseudo-mode $F^{(\nu)}$ and use the eigenmodes to obtain an estimate

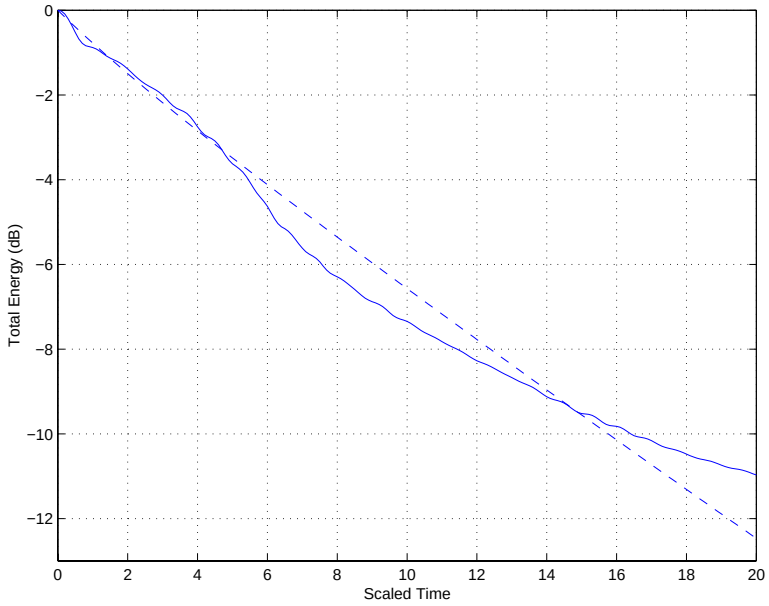

Figure 6: Energy curves for $K = L = 10$, pseudo-modes (solid), eigenmodes (dashed).

to the correlation matrix and total energy without the need to integrate (31). We illustrate this as follows.

Let ψ^ν be the eigenvector of A associated with the eigenvalue μ^ν, that is,

$$A\psi^\nu = \mu^\nu \psi^\nu.$$

Then the solution of

$$\dot{\mathcal{F}}^\nu(t) = A\,\mathcal{F}^{(\nu)}(t), \qquad \mathcal{F}^{(\nu)}(0) = \psi^\nu, \tag{38}$$

is $\mathcal{F}^{(\nu)}(t) = \exp(\mu^\nu t)\ \psi^\nu$. We call $\mathcal{F}^{(\nu)}$ an eigenmode. Now we can use the set of eigenmodes $\{\mathcal{F}^{(\nu)}(t)\}_{\nu\in\mathcal{N}}$ to calculate an estimate to the correlation matrix and the expected total energy. The dashed curve in Figure 6 represents the normalized energy calculated using the eigenmodes $\{\mathcal{F}^{(\nu)}(t)\}_{\nu\in\mathcal{N}}$.

From Figure 5 we observe that the energy exchange with sufficiently high frequencies is negligible. This indicates that it is not necessary to choose very large values of K and L. In Figure 7 we compare the total energy values for $K = L = 10$ with M = N = 10 (solid) and $K = L = 20$ with $M = N = 20$ (dotted). As can be seen, the differences are negligible.

Finally, note that the step function on each cell $[k, k+\Delta k] \times [l, l+\Delta l]$ in the frequency domain corresponds

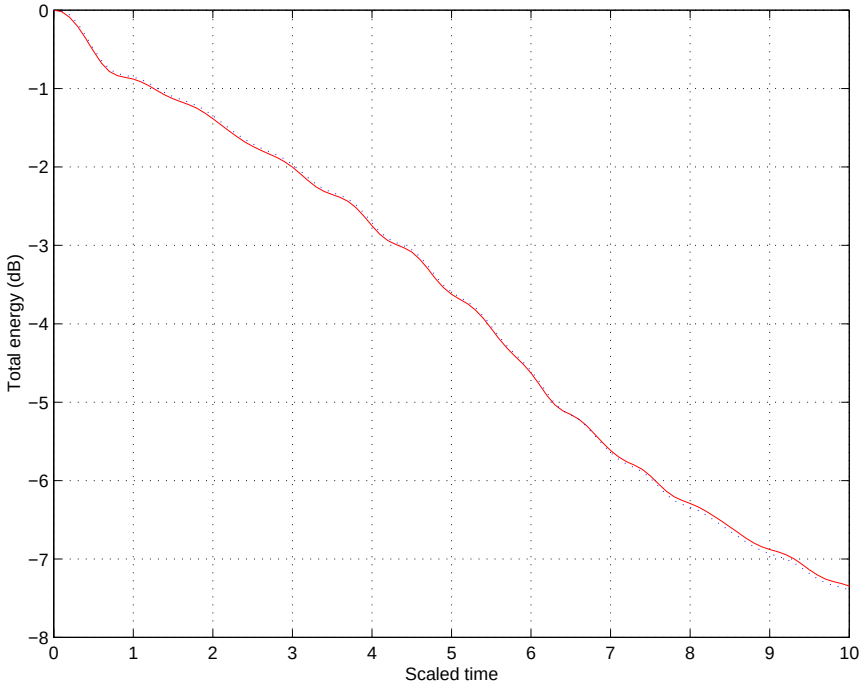

Figure 7: Comparison of Energy curve for $K = L = 10$ (solid) and $K = L = 20$ (dotted).

to

$$\begin{aligned}
\phi_{kl}(x,y) &= \frac{1}{\pi^2}\int_0^\infty\int_0^\infty \chi_{kl}(\alpha,\beta)\,\cos(\alpha x)\,\cos(\beta y)\,d\alpha\,d\beta \\
&= \frac{1}{\pi^2}\int_k^{k+\Delta k}\int_l^{l+\Delta l} \cos(\alpha x)\,\cos(\beta y)\,d\alpha\,d\beta \\
&= \frac{\Delta k\Delta l}{\pi^2}\,\mathrm{sinc}\left(\frac{\Delta k}{2}x\right)\,\cos\left(\left[k+\frac{\Delta k}{2}\right]x\right)\,\mathrm{sinc}\left(\frac{\Delta l}{2}y\right)\,\cos\left(\left[l+\frac{\Delta l}{2}\right]y\right),
\end{aligned}$$

in the physical domain, where $\mathrm{sinc}\ x = \frac{\sin x}{x}$. Thus if smaller Δk and Δl are chosen, the magnitude of ϕ_{kl} is dispersed over a large area and leads to the smaller scale interaction of the sound field. Therefore, we must choose an appropriate cell size Δk and Δl in order to admit a desired scale interaction. For example, if the spatial domain is bounded by rigid walls of size L_x and L_y, then $\Delta k = \frac{\pi}{L_x}$ and $\Delta l = \frac{\pi}{L_y}$.

We remark that questions of convergence to a stable system as $N, M \to \infty$ in the problems discussed here are not particularly relevant. More precisely, the margin of stability of the original system (5)-(6) is zero. In fact, it is observed in our calculations that the distribution of eigenvalues in Figure 3 is shifted toward the imaginary axis by every doubling of N, M. One can employ our algorithm in a more practical setting by restricting the

computational domain (i.e., the model) to a finite cavity with weak boundary damping. This yields an acoustic problem with a fixed margin of stability for which questions of limiting behavior as $N, M \to \infty$ are relevant (e.g., see [2]).

9 Concluding Remarks

The above discussions constitute our initial contributions toward the effective use of an array of microacoustic actuators as an absorbing surface for enclosed acoustic cavities. We formulated an approximate time domain initial-boundary value problem for a distributed parameter system for the acoustic energy due to propagation of an initial random field. Modeling the cavity as a half-plane, we derived the corresponding frequency domain model and the resulting expressions for autocorrelation for the sound field, including the pressure field, the velocity field, and the total energy.

We then developed semi-discrete finite element approximations based on piecewise constant elements (zero order splines) for these expressions and illustrated their use with sample calculations.

We believe the computational methods discussed in this paper can provide useful tools for predicting the performance of a given actuator array with respect to a given band of frequencies. This information can in turn be used in optimal design of such arrays.

Acknowledgments

This research was supported in part by the US Air Force Office of Scientific Research under grant AFOSR F49620-01-1-0026, in part by the Fulbright Scholar Program, in part by King Fahd University of Petroleum and Minerals through a Sabbatical Leave Program, and in part by the Thomas Lord Research Center, Cary, N.C.

References

[1] A. O. Andersson. Fluidic element noise and vibration control constructs and methods. European Patent Office, EP0829848, www.european-patent-office.org, 1998.

[2] H. T. Banks, K. Ito, and C. Wang. Exponentially stable approximations of weakly damped wave equations. In *DPS Control and Applications*, Birkhauser Intl. Ser. Num. Math, Volume 100, pages 1–33. 1991.

[3] R. K. Cook, R. V. Waterhouse, R. D. Berendt, S. Edelman, and J. M. C.T̃hompson. Measurement of correlation coefficients in reverberant sound fields. *J. Acoust. Soc. Am.*, 27(6):1072–1077, 1955.

[4] D. G. Crighton, A. P. Dowling, J. E. F. Williams, M. Heckl, and F. G. Leppington. *Modern Methods in Analytical Acoustics*. Springer-Verlag, London, 1992.

[5] M. Furstoss, D. Thenail, and M. A. Galland. Surface impedance control for sound absorption: Direct and hybrid passive/Active strategies. *J. Sound Vib.*, 203(2):219–236, 1997.

[6] K. U. Ingard. *Notes on Sound Absorption Technology*. Noise Control Foundation, Poughkeepsie, NY, 1994.

[7] L. E. Kinsler, A. R. Frey, A. B. Coppens, and J. V. Sanders. *Fundamentals of Acoustics*. John Wiley & Sons, Inc., New York, 1982.

[8] C. J. Mazzola. Active piston sound absorber. *Intelligent Materials and Systems*, pages 165–173, 1995.

[9] C. T. Morrow. Point-to-point correlation of sound pressures in reverberation chambers. *J. Sound Vib.*, 16(1):29–42, 1971.

[10] P. M. Morse and K. U. Ingard. *Theoretical Acoustics*. Princeton University Press, Princeton, NJ, 1968.

[11] H. F. Olson and E. G. May. Electronic sound absorber. *J. Acoust. Soc. Am.*, 25(6):1130–1136, 1953.

[12] R. V. Waterhouse. Statistical properties of reverberant sound fields. *J. Acoust. Soc. Am.*, 43(6):1436–1444, 1968.

[13] E. G. Williams. *Fourier Acoustics: Sound Radiation and Nearfield Acoustical Holography*. Academic Press, San Diego, California, 1999.

[14] R. W. Young. Sabine reverberation equation and sound power calculations. *J. Acoust. Soc. Am.*, 31(7):912–921, 1959.